

Article

Optimal Mixture Designs for Heavy Metal Encapsulation in Municipal Solid Waste Incineration Fly Ash

Ying Wang ¹ , Wen Ni ^{2,*}, Siqi Zhang ², Jia Li ³ and Prannoy Suraneni ¹

¹ Department of Civil, Architectural, and Environmental Engineering, University of Miami, Coral Gables, FL 33146, USA; yxw1218@miami.edu (Y.W.); suranenip@miami.edu (P.S.)

² School of Civil and Resources Engineering, University of Science and Technology Beijing, Beijing 100083, China; zsq2017@ustb.edu.cn

³ School of Energy and Environment Engineering, University of Science and Technology Beijing, Beijing 100083, China; s20180177@xs.ustb.edu.cn

* Correspondence: niwen@ces.ustb.edu.cn; Tel.: +86 13520195371

Received: 17 September 2020; Accepted: 2 October 2020; Published: 4 October 2020



Abstract: Mixing municipal solid waste incineration fly ash (MSWIFA) with industrial by-products such as ground granulated blast furnace slag (GGBFS) and ladle furnace slag (LFS) can lead to a hardened system which can encapsulate the heavy metals present in the MSWIFA. The objective of this study is to find optimal mixture designs to effectively encapsulate these heavy metals. The nature of the hydrates and the strength of the mixtures are studied to develop a sustainable and practical construction material incorporating MSWIFA. Heavy metals including Cr, Cu, Zn and Cd are safely encapsulated in several developed mixtures with leachate concentration below EPA drinking water limit. The encapsulation behavior is complex and depends on metal type, age of testing, and hydration products. In general, mixtures containing LFS have more aluminate hydrates, and show greater encapsulation capacity for most heavy metals. However, they also generally show significant Sb leaching. Mixtures which show satisfactory encapsulation for all ions and adequate strength development are identified. Three ideal mixtures, including one containing zero cement, are identified which satisfy both leaching and strength requirements.

Keywords: municipal solid waste incineration fly ash; ladle furnace slag; Friedel's salt; heavy metal encapsulation

1. Introduction

Municipal solid waste incineration fly ash (MSWIFA) is classified as hazardous waste in numerous locations across the globe [1–5]. MSWIFA has high concentrations of soluble heavy metals, including Pb, Zn, Cr, Sb, Hg, Cu, Ni, and Cd. Therefore, the MSWIFA is a hazardous pollutant when considering environmental risk control [6]. Solidification, which can be defined as the use of a binder, which either chemically or physically binds toxic waste matter to prevent leaching is a recognized way to dispose of MSWIFA [7,8]. Solidification processes using Portland cement have received significant attention and the encapsulation ability of cement hydrates including ettringite and C-S-H has been reviewed in the literature [6,9]. The relatively high CO₂ emissions associated with Portland cement have led to the development of numerous more sustainable alternatives with low or zero cement content [10]. Such alternatives have the added advantage of using industrial by-products, which are often otherwise landfilled. The objective of this work is to critically evaluate and develop a sustainable binder material using ground granulated blast furnace slag (GGBFS), ladle furnace slag (LFS), and flue gas desulfurization (FGD) gypsum that can encapsulate the heavy metals in MSWIFA.

GGBFS is a commonly used and well-known supplementary cementitious material for concrete. It has often been used as a component in mixtures for heavy metal encapsulation [10–19]. LFS is a lesser known material and a by-product of steel manufacture which typically has both amorphous and crystalline phases with large amounts of aluminum and calcium [20]. Although the composition and crystalline phase in LFS tend to be variable, a commonly found crystalline phase in LFS is mayenite ($C_{12}A_7$). In our previous work, we have investigated mayenite reactions and found that it can form Friedel's salt when it reacts with the chloride that is commonly present in MSWIFA [21]. Friedel's salt is a layered double hydroxide (LDH) material, with interesting anion-exchange properties which leads to a potential for high heavy metals encapsulation [21]. Due to these characteristics and potential hydrates that are formed with LFS, its use for heavy metal encapsulation warrants further study.

The hypothesis of this work is that the use of GGBFS, LFS, and MSWIFA will lead to a binder that has significant amount of LDH formation, which will lead to a system that is sustainable, strong, and which will encapsulate the heavy metals in MSWIFA. While the specific systems studied here have not been investigated in the past, the hypothesis is in line with the literature which suggests that the use of such slags will favor the formation of hydrates and microstructures that will result in enhanced immobilization of heavy metals [22]. This work is part of a larger study on sustainable by-product binders and results on chloride binding and hydration in some of the systems studied here have been already published [21].

2. Materials and Methods

2.1. Materials

The MSWIFA was obtained from a local municipal waste incineration plant in Beijing, China. The FGD gypsum and GGBFS were obtained from Xingtai, China. The LFS was collected from Liuzhou, China. The GGBFS is classified as Grade S95 according to GB/T 18046-2008 [13]. Grade S95 slags provide compressive strength values at 7 days of at least 75% of a control mixture, and 28-day values of at least 95% of the control mixture. A Type I ordinary Portland cement (OPC) was also used in this study. The chemical compositions of all materials were determined using X-ray fluorescence (XRF), following procedures similar to ASTM C 114-18. ASTM C204-18 was used to determine the Blaine fineness of all materials. The fineness and chemical composition are shown in Table 1.

Table 1. Chemical composition (mass %) and Blaine fineness (m^2/kg) of the raw materials [21].

Material	CaO	SiO ₂	Al ₂ O ₃	MgO	Fe ₂ O ₃	Na ₂ O	K ₂ O	SO ₃	Cl	Blaine Fineness
GGBFS	46.54	29.78	12.18	6.00	1.22	0.45	0.41	0.36	0.02	420
LFS	55.86	0.73	36.91	3.40	1.16	0.00	0.01	0.40	0.09	400
MSWIFA	43.82	3.80	1.09	2.64	4.53	5.75	7.63	8.56	17.4	913
Gypsum	48.13	2.62	0.96	1.48	0.48	0.08	0.21	44.03	0.43	373
Cement	64.05	22.87	4.47	2.46	3.48	0.52	-	2.44	0.011	341

When considering the chemical composition, GGBFS and LFS both contain high CaO contents. GGBFS contains a moderate amount of Al₂O₃ and a large amount of SiO₂. The LFS has a large amount of Al₂O₃ and a negligible amount of SiO₂. This composition is somewhat different from other LFS materials found in the literature and appears to be because Al bars were used in process of extraction and purification of steel [20,21]. MSWIFA contains considerable amounts of Cl, SO₃, K₂O, Na₂O and a large amount of CaO.

The reactivity of the slags and MSWIFA was assessed and the results suggest that the GGBFS and the LFS are latent hydraulic materials and the MSWIFA is an inert material [15]. The LFS however causes strength reductions when used in cement paste, likely because the mayenite causes sulfate imbalance [15].

X-ray diffraction (XRD) patterns of all materials are shown in Figure 1. The procedure followed for XRD is similar to that described in detail in Section 2.3. As expected, the GGBFS is mostly amorphous, though it does show minor amounts of jaffeite and fukalite. The LFS is also largely amorphous, but it shows substantial amounts of mayenite. On the other hand, the MSWIFA is largely or completely crystalline. It shows the presence of numerous crystalline phases, including calcium sulfates, sodium sulfate, sodium chloride, etc. The crystalline phases detected in the tested materials are in agreement with findings from the literature [15,23,24]. However, we note here that MSWIFA can be a very variable material in terms of its bulk oxide composition and crystalline phases, and generalizations regarding its chemistry should be done with caution.

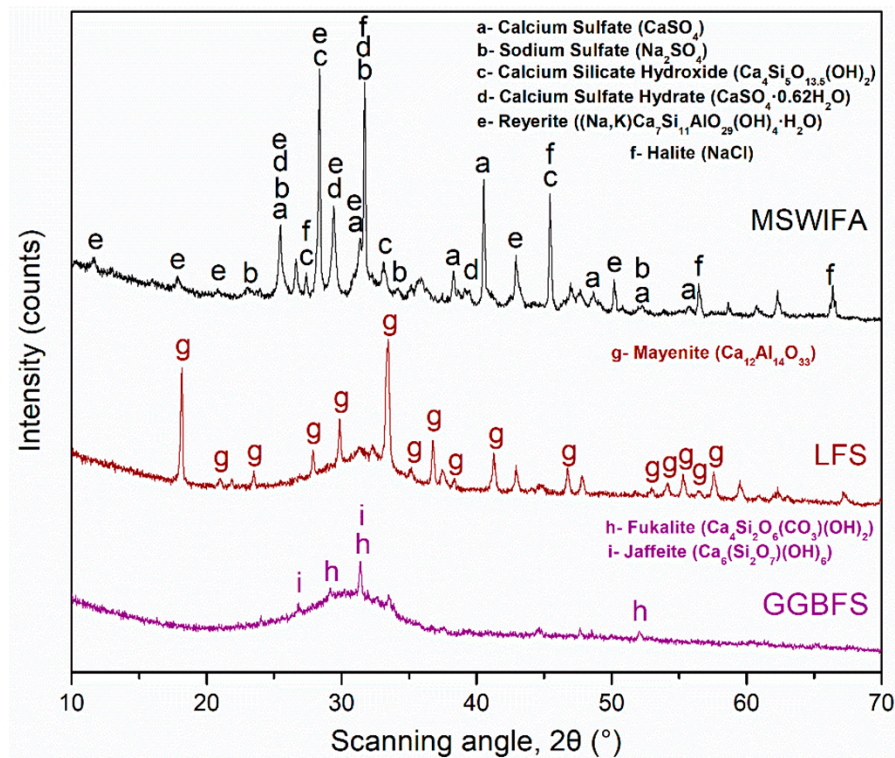


Figure 1. X-ray diffraction (XRD) patterns for MSWIFA, LFS, and GGBFS [16,22] (PDF#: calcium sulfate—37-1496; sodium sulfate—37-1465; calcium silicate hydroxide—29-0381; calcium sulfate hydrate—41-0225; reyerite—29-1039; halite—05-0628; mayenite—48-1882; fukalite—29-0308; jaffeite—46-1285).

The phase composition of the cement as provided by the manufacturer is C₃S: 56.54; C₂S: 20.87; C₃A: 6.22; C₄AF: 10.31 (all amounts in mass %). Further details on the raw materials and their characterization are provided elsewhere [15,21].

2.2. Mixture Design

The 14 paste mixtures that were tested in this study are shown in Table 2. The mixtures were divided into four groups: CB (variable amounts of cement and GGBFS), BM (variable amounts of MSWIFA and GGBFS), LB (variable amounts of LFS and GGBFS) and GB (variable amounts of gypsum and GGBFS). The notation C70B0 refers to a mixture with 70% cement and 0% GGBFS; other notations can be interpreted similarly. Each group has three to four mixtures, and in these mixtures the sum of the amounts of the first and second component is constant, and one decreases as the other increases. In groups LB and GB, the MSWIFA content was constant at 30% of the total solids. In group CB, the MSWIFA was constant at 20% and in group BM, the MSWIFA amount varies from 20% to 60%. Cement and GGBFS amounts range from 0% to 70%, LFS amounts range from 0% to 60%, MSWIFA amounts

range from 20% to 60%, and gypsum amounts range from 2% to 14%. The water-to-binder ratio (w/b) was maintained at 0.30 for group CB and BM, where binder is the sum of the masses of GGBFS, MSWIFA, LFS, gypsum, and the cement. However, due to poor workability, the water-to-binder ratio for group LB and GB was maintained at 0.40. These mixture designs were based on the results of preliminary experiments and provide a range of compositions containing MSWIFA, GGBFS, LFS, cement and gypsum which are anticipated to provide systems with a range of hydrates.

Table 2. Mixture designs used in the study (in mass %); water/binder is unitless [21].

Mixture	MSWIFA	GGBFS	LFS	Gypsum	Cement	Water/Binder Ratio
C70B0	20	0	0	10	70	0.3
C56B14	20	14	0	10	56	0.3
C42B28	20	28	0	10	42	0.3
C28B42	20	42	0	10	28	0.3
B70M20	20	70	0	10	0	0.3
B50M40	40	50	0	10	0	0.3
B30M60	60	30	0	10	0	0.3
L0B60	30	60	0	10	0	0.4
L20B40	30	40	20	10	0	0.4
L40B20	30	20	40	10	0	0.4
L60B0	30	0	60	10	0	0.4
G14B16	30	16	40	14	0	0.4
G6B24	30	24	40	6	0	0.4
G2B28	30	28	40	2	0	0.4

2.3. Experimental Methods

The materials were mixed mechanically in a mixer according to ASTM C305-14 [15,21]. The fresh paste was then cast into 5-cm cubic molds after tamping and vibration [15,21]. Pastes were demolded at one day, and then cured at temperature of 30 ± 2 °C and a relative humidity of 95%. The temperature of 30 °C was used to accelerate hydration and strength processes, which is an important consideration for non-cement mixtures. Three specimens were cast for each mixture, and the curing times were 3, 7, 28, and 90 days for group LB and GB, with an extended curing time for groups CB and MB until 180 days. The compressive strength test was performed according to ASTM C109-20a on all pastes at 3, 28, and 90 days in order to determine the strength evolution.

Broken pieces of paste were stored in absolute ethyl alcohol for 2 days to stop hydration. After 2 days, filtration was performed, followed by drying under vacuum at 40 °C for 1 day [24]. The pieces were then ground and sieved through a 45- μ m mesh and the resulting powder was used for XRD and leaching tests. XRD was performed at 3, 7, and 28 days to determine the nature of the hydrates formed in the different mixtures in a qualitative manner. The scanning was performed from 3° to 90° 2 θ and the device was operated at 40 kV and 40 mA and had a Cu K α anode. Leaching tests were performed based on ASTM D8155-17 at 3, 7, 28, 90, and 180 days to evaluate the extent of encapsulation of the heavy metals in the MSWIFA. Around 10 g of powder samples was mixed with 100 mL of deionized water in a closed conical flask. Then, the flask was placed on a shaking table at 23 °C for 8 h and it was shaken at 110 rpm and then allowed to rest for 16 h. The leachate was filtered with a 0.45- μ m membrane filter at the end of the extraction. The concentration of heavy metals in the leachate was detected by inductively coupled plasma mass spectrometry (ICP-MS). While the leached concentrations of heavy metals, sulfate, and chloride were all measured, only data for heavy metals are reported here in detail. The chloride encapsulation is discussed in detail elsewhere [21]. ICP-MS was also run on an MSWIFA–water mixture under the same conditions. Under these conditions, the MSWIFA had very high leached amounts (C_0), and the concentrations of many of the heavy metals were higher than the

EPA drinking water limitation. The concentration of heavy metals was determined for given mixtures and heavy metals (C_x), and the encapsulation percentage (E) for each heavy metal was obtained using Equation (1) [21]:

$$E = \left(1 - \frac{C_x}{P \times C_0}\right) \times 100 \quad (1)$$

where C_x is the mixture leachate concentration, P is the mass proportion of MSWIFA in the paste, and C_0 is the leachate concentration in the MSWIFA and water mixture.

It is noted here that strength testing is performed at three ages (3, 28, and 90 days), XRD is performed at three ages (3, 7, and 28 days), and leaching is performed at five ages (3, 7, 28, 90, and 180 days). These differences arise due to practical difficulties and labor associated with testing of several different mixtures. As the main focus of this work is on leaching, it is tested most frequently. Regardless, the testing regime is extensive and allows us to clearly identify the changes in the material behavior over time.

3. Results and Discussion

3.1. Compressive Strength Evolution

The compressive strength evolution of the mixtures during 90 days of hydration is provided in Figure 2. Three replicate paste cubes were tested at each age. They generally showed less than 5% coefficient of variability in the values of the strength. The strengths increase over time, though the rates of increase and the values vary depend on the mixture design. The early age strength of the LB and GB groups is very low, with 3-day values lower than 10 MPa. However, these groups show a sharp increase in strength from 3 to 28 days and the strength keeps increasing from 28 to 90 days. In terms of the 3- and 28-day strength, C28B42 has the largest values of 46 MPa and 52 MPa, respectively. Apart from the LB and GB groups, mixtures B30M60 and B50M40 also show low early strength. Low early strengths occur when there are high amounts of MSWIFA or LFS in the mixtures; strength generally decreases as the amounts of MSWIFA or LFS increase. For MSWIFA, strength reductions are caused due to its inert nature (no amorphous content and no reaction in cementitious systems) in addition to the deleterious species in the ash (including chloride, sulfate, and metallic aluminum [15,21]). The negative effects of LFS are likely due to the presence of mayenite which can cause flash set and affect sulfate balance, apart from impeding later age reactions and causing conversion phenomena [13,20,21,25,26].

Mixtures with high amounts of cement and GGBFS gain the most strength in both short- and long-term hydration. As the amount of cement decreases and the amount of GGBFS increases, the strength first increases and then decreases at later ages. This suggests that there is an optimal balance between cement and GGBFS (42% cement and 28% GGBFS) for later age strength. This is because of the highly reactive nature of the GGBFS, which will continue to react in cementitious systems, even at later ages, which reduces the porosity and result in the strength increasing [10]. As the amount of LFS increases, the strength decreases at 90 days, when compared to mixtures with lower amounts of LFS. Gypsum does not appear to have an obvious impact on the strength evolution.

3.2. Hydrate Evolution

Figure 3 shows the XRD patterns of seven representative pastes hydrated for 3, 7, and 28 days. These mixtures are chosen so they provide an overall picture of the hydration of all pastes in order to keep this work concise. For different mixture designs, the main hydration products include ettringite ($\text{Ca}_6\text{Al}_2(\text{SO}_4)_3(\text{OH})_{12} \cdot 26\text{H}_2\text{O}$), Friedel's salt ($\text{Ca}_4\text{Al}_2\text{O}_6\text{Cl}_2 \cdot 10\text{H}_2\text{O}$), sturmanite ($\text{Ca}_6\text{Fe}_2(\text{SO}_4)_2[\text{B}(\text{OH})_4](\text{OH})_{12} \cdot 26\text{H}_2\text{O}$), C-S-H, and calcium magnesium aluminum oxide silicate (C-S-A-M). A small amorphous hump appears in mixtures with higher GGBFS and cement contents. The XRD peak heights are used only as a qualitative indicator as they are affected by numerous factors. The discussion below, based on peak heights, is only intended to provide a relative estimate of the hydrate amounts.

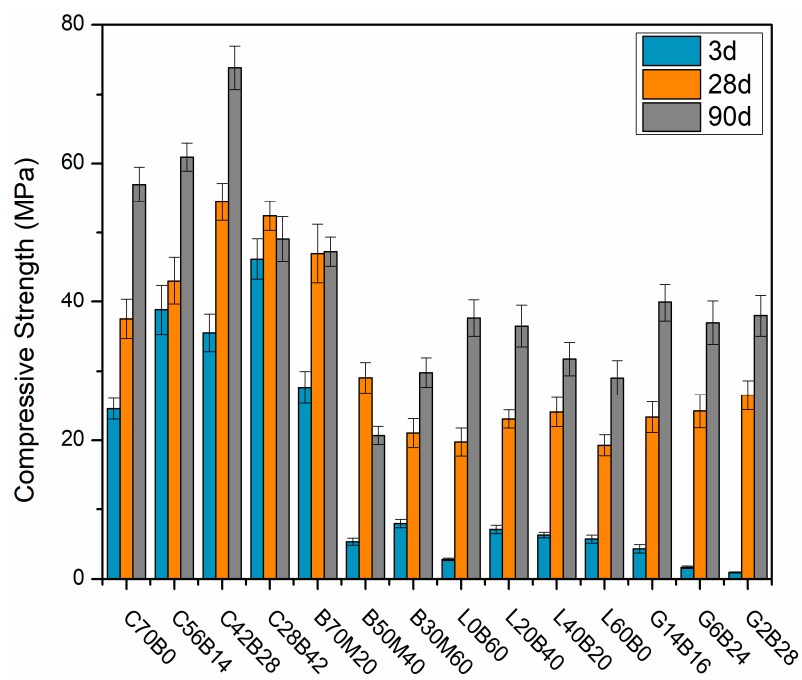


Figure 2. Compressive strength evolution of all mixtures during the 90-day period. Error bars are equal to one standard deviation of the mean on each side.

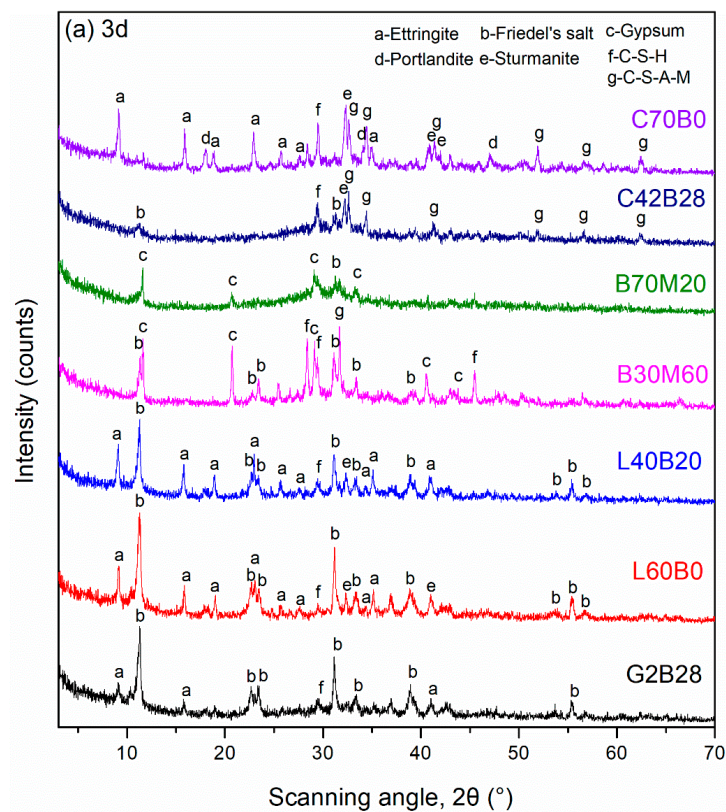


Figure 3. Cont.

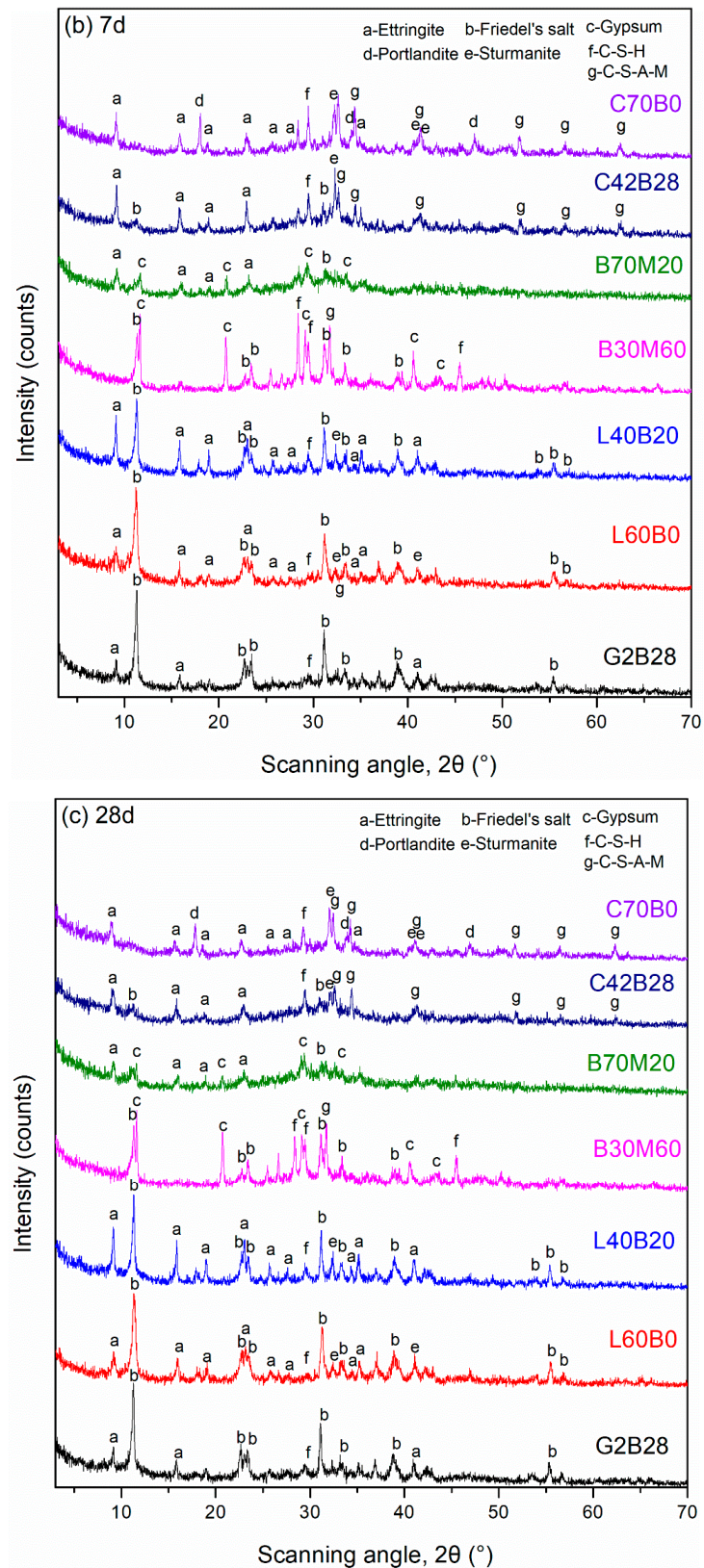


Figure 3. XRD patterns for pastes hydrated for (a) 3 days, (b) 7 days, and (c) 28 days for chosen groups (PDF#: ettringite—41-1451; Friedel's salt—31-0245; gypsum—21-0816; portlandite—72-0156; sturmanite—35-0637; C-S-H—14-0035; C-A-S-M—13-0272).

At 3 days, there is no ettringite in C42B28, B30M60 or B70M20, however, ettringite is formed in the cement paste without GGBFS (C70B0), suggesting that GGBFS impedes the formation of ettringite at early ages [27]. At 3 days, Friedel's salt and gypsum peaks are the most intense in L0B60, while no ettringite peaks are found. At later ages, the ettringite peaks increase in intensity whereas gypsum and Friedel's salt peaks decrease in intensity. This is probably because of the reaction between sulfates, GGBFS, and Friedel's salt forming ettringite [21]. With larger LFS amounts, the aluminum coming from $C_{12}A_7$ has a greater chance to react with Cl^- , forming Friedel's salt before ettringite can form [20,21,26]. Conversion mechanisms and ionic exchange may also occur between Friedel's salt and ettringite, which may explain the inverse relationship between the amounts of these two phases [21]. After 7 days, all pastes show the presence of ettringite except B30M60, which has large amounts of MSWIFA. This may be due to the excessive Cl^- in the system impeding Friedel's salt transformation to ettringite. When there is LFS in the system, Friedel's salt and ettringite will form and remain stable. There are no obvious changes in the peak heights of LFS-containing systems during the hydration process, possibly because that the system has abundant amounts of tetrahedrally coordinated Al and SO_4^{2-} which results in relatively stable amounts of Friedel's salt and ettringite. Ettringite decreases at later ages when there is cement in the system, possibly due to the transformation to monosulfate phases. With excessive MSWIFA, there are large amounts of gypsum in B30M60. Only small amounts of gypsum and ettringite are seen in the mixture G2B28, which has a small amount of gypsum to start with. These changes over 3 to 28 days for the different mixtures are summarized in Table 3.

Table 3. Qualitative changes in amount of hydrates of representative mixtures. The notations are as follows—√: Is present; ×: Is absent; ↑: Increases; ↓: Decreases.

Mixture	Ettringite			Friedel's salt			Gypsum			Sturmanite			C-S-H and C-S-A-M		
	3d	7d	28d	3d	7d	28d	3d	7d	28d	3d	7d	28d	3d	7d	28d
C70B0	√	↓			×			×		√	↓		√		↓
C42B28	×	√	↓		×			×		√	↑	↓			√
B70M20	×	↑			×		√	↓			×				×
B30M60		×			√			√			×		√		↓
L40B20	√	↑		√	↑			×		√	↑		√		↑
L60B0	√	↓		√	↑			×			√				√
G2B28		√			√			×			×				√

3.3. Heavy Metal Leaching

3.3.1. MSWIFA and Water Mixture

Figure 4 shows the concentration of heavy metals in the leachate of MSWIFA mixed with water at a liquid-to-solid ratio of 10, and the corresponding EPA drinking water limits. The concentrations of several metals are close to or higher than EPA limits. If MSWIFA is landfilled without any treatment, it may lead to severe pollution, specifically for Cr, Pb and Cd, which show concentrations above the EPA drinking water limit. The worst behavior is seen with Pb, with a concentration 1350 times greater than the limit. The concentrations of Zn and Hg approach the limit, and they may exceed it under more concentrated conditions. To landfill such hazardous material without any treatment clearly poses a significant pollution risk.

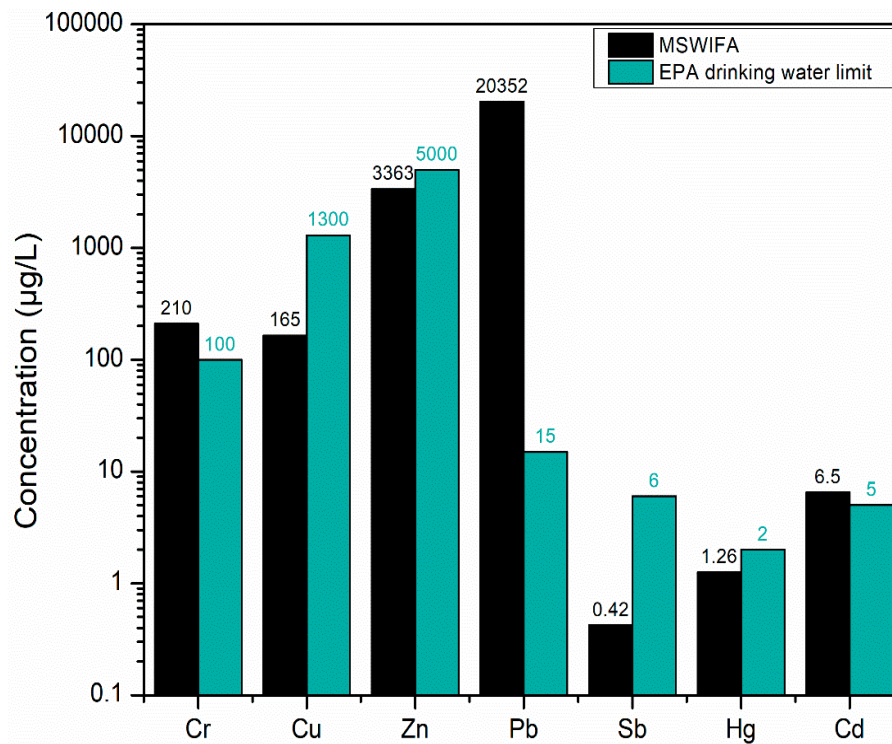


Figure 4. Concentrations of MSWIFA powder leachate and EPA drinking water limit. In the rest of this section, the encapsulation of each heavy metal is discussed.

3.3.2. The Encapsulation of Cr

Figure 5 shows the Cr concentrations and the encapsulation percentage at all ages for all groups. All mixtures significantly reduce Cr concentrations, and the Cr amounts are always below the EPA drinking water limit, in contrast to the MSWIFA and water mixture, where the Cr amount is double the limit. The LB and GB groups show greater Cr encapsulation than the other groups, with the encapsulation percentage above 90%. The BM and CB groups show somewhat lower Cr encapsulation, with the percentage ranging from −14% to 90% at 28 days. A negative value of encapsulation here and for other ions is likely caused because of the very small concentrations, sometimes below 1 µg/L, and small errors may cause negative encapsulation percentages. The encapsulation increases with time, and at 180 days, for all mixtures except one (B30M60), the encapsulation is over 89%. These findings suggest that the LFS increases Cr encapsulation at early and later ages, likely due to high amounts of calcium aluminate hydrates, ettringite and Friedel's salt in the mixtures with LFS. In mixtures without LFS, the encapsulation process is slower. The Cr encapsulation mechanism may be explained using the literature [6,9–11,22,24,28–36]. It is known that calcium sulfoaluminate hydrates play an exceptional role as Cr immobilizers. Cr can partially replace the aluminum in ettringite [22] and can also be integrated into the Friedel's salt layers, either through ionic substitution or by surface adsorption [9,10,24,34–36]. Cr can also be incorporated into the C-S-H as insoluble chromium hydroxides [6,32].

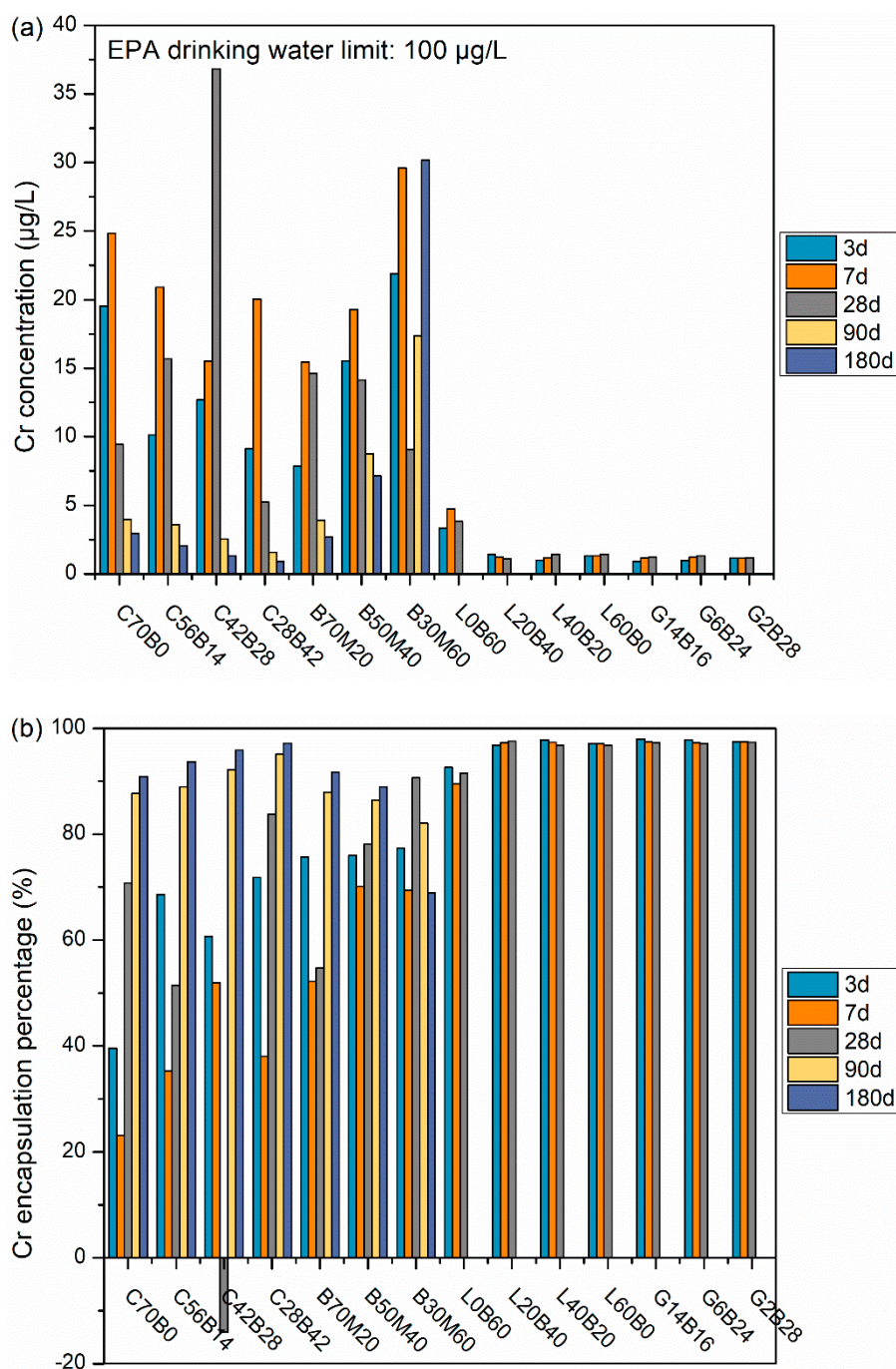


Figure 5. The (a) Cr concentration and (b) encapsulation percentage for the leachate in all groups at all ages.

3.3.3. The Encapsulation of Cu

All mixtures show Cu amounts significantly below the EPA drinking water limit (Figure 6), but it should be noted that this is also the case with the MSWIFA and water mixture. The encapsulation percentages of LB and GB groups are above 47%, while for B70M20 and group CB, the values range from −166% to 10% at 28 days. For the mixtures, the encapsulation percentage first reduces and then increases. This reduction happens at 7 days for groups LB and GB, and at 28d for groups BM and CB. Groups with LFS show faster and greater encapsulation, like with Cr. For the BM and CB groups, the percentage is above 83% at 180 days. The literature [18,35,37] suggests that copper hydroxide could

be the dominant species that is formed during hydration and it is physically encapsulated in the C-S-H gel, but Cu can also be fixed in ettringite and Friedel's salt by ionic substitution and adsorption [35].

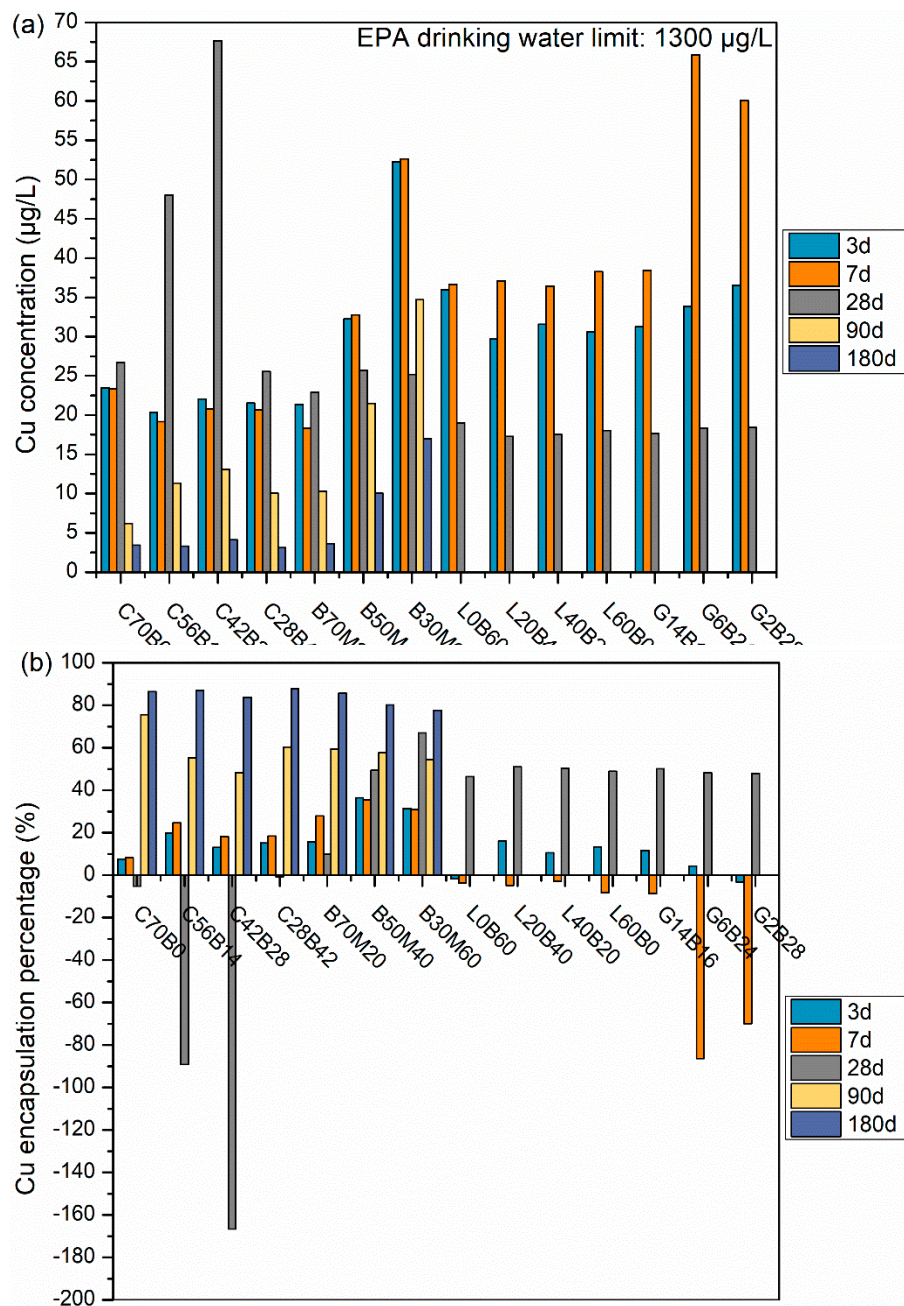


Figure 6. The (a) Cu concentration and (b) encapsulation percentage for the leachate in all groups at all ages.

3.3.4. The Encapsulation of Zn

The Zn concentrations and the encapsulation percentage values are shown in Figure 7. All mixtures show Zn amounts orders of magnitude lower than the EPA drinking water limit, in contrast with the MSWIFA and water mixture, which showed values somewhat comparable with the limit. This suggests that all groups strongly encapsulate Zn (encapsulation percentages all over 97%). For groups BM and CB, the concentration of the leachate first reduces and then increases during the hydration time from 3 to 180 days. Generally, groups with LFS show slightly greater encapsulation than groups without. Zn encapsulation mechanisms in this study can be explained based on the literature [6,11,29,32,35,37,38].

During the hydration process, Zinc forms hydroxides at high pH conditions (>8) [38]. The anionic nature of these hydroxides prevents their adsorption onto the negatively charged C-S-H surface, but they can form the complex $\text{CaZn}_2(\text{OH})_6 \cdot \text{H}_2\text{O}$ [32,37] or become otherwise physically encapsulated in the bulk. Others have postulated that the Zn could be fixed in a metallic C-S-H phase [37].

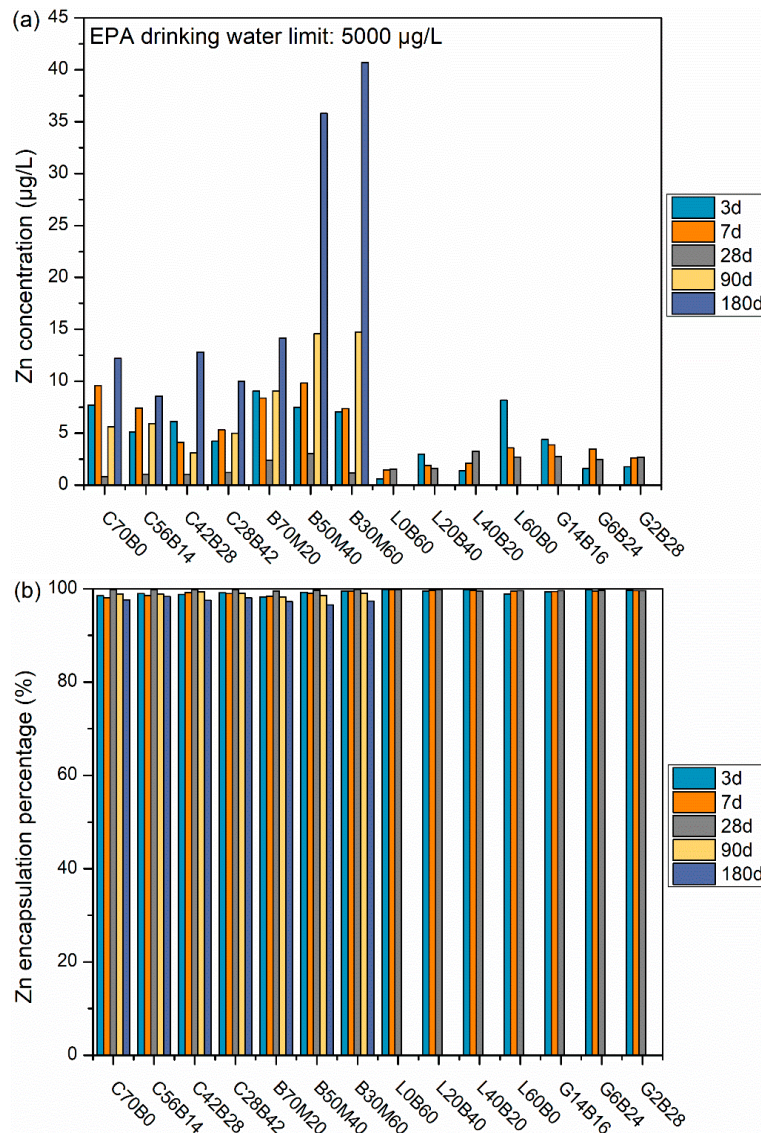


Figure 7. The (a) Zn concentration and (b) encapsulation percentage for the leachate in all groups at all ages.

3.3.5. The Encapsulation of Pb

All mixtures except one show Pb amounts below the EPA drinking water limit (Figure 8), in contrast with the MSWIFA and water mixture, which shows values three orders of magnitude greater than the limit. The exception is the mixture C70B0 which exceeds the EPA drinking water limit (which is 15 $\mu\text{g/L}$) at all ages from 3 to 180 days. This finding implies that a mixture with cement and gypsum cannot encapsulate Pb to the required levels [16]. All groups encapsulate Pb very well, with encapsulation percentages above 99%. Pb encapsulation performance is in agreement with the literature [1,6,8–11,22,32,36–43]. Pb is known to be an amphoteric element, so Pb concentration is high under highly alkaline conditions (such as in C70B0), but low in more neutral conditions. Pb is not fixed within the C-S-H, but it can be adsorbed on the C-S-H surface. It is difficult to achieve

efficient Pb immobilization using only cement [1,9,10,22,32,36]. Pb is mostly stabilized through physical encapsulation of its precipitates by the hardened hydrate matrix [10].

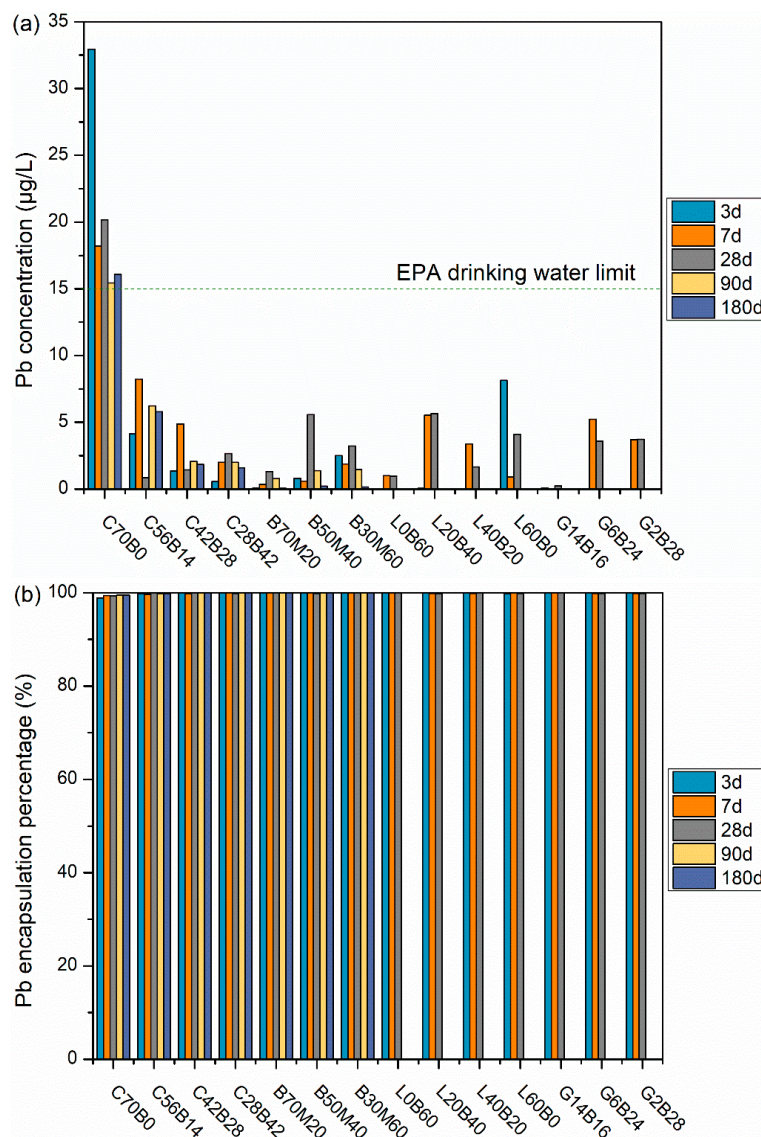


Figure 8. The (a) Pb concentration and (b) encapsulation percentage for the leachate in all groups at all ages. The EPA drinking water limit is shown in the concentrations figure as a dotted line; however, this is not done for all heavy metals. It is only done when the metal concentrations and EPA limit are somewhat comparable.

3.3.6. The Encapsulation of Sb

In Figure 9, the concentrations and encapsulation percentage of Sb are shown. For all groups, there is no encapsulation; instead Sb leaches from the system. Several mixtures, including L20B40, L40B20, and L60B0 do not meet the EPA drinking water limit. The MSWIFA–water mixture meets the EPA drinking water limit. Unlike for other ions, where occasional negative values are observed in the encapsulation percentage, almost all mixtures show high negative encapsulation percentages. These numbers suggest that the negative values here are due to a lack of Sb encapsulation in these mixtures. Mixtures with LFS potentially result in Sb transforming to soluble ions in forms such as $\text{Sb}(\text{OH})_6^-$. Sb forms oxyanions and the higher leachability of these oxyanions is correlated to the alkaline conditions in these mixtures [29,44–47]. Physical encapsulation is generally the dominant

mechanism for Sb immobilization [44]. It is postulated that the porosity of mixtures in groups LB and GB is greater than the mixtures in groups CB and BM, based on the strength evolution shown in Figure 2. Due to the porosity, the high alkaline conditions, and freely soluble Sb, the Sb will leach out from the mixture. The higher Al content within the LFS systems, could also lead to a negatively charged three-dimensional amorphous Si-O-Al structure [45]. The Sb oxyanions may release from these structures because of the more unbalanced charge conditions.

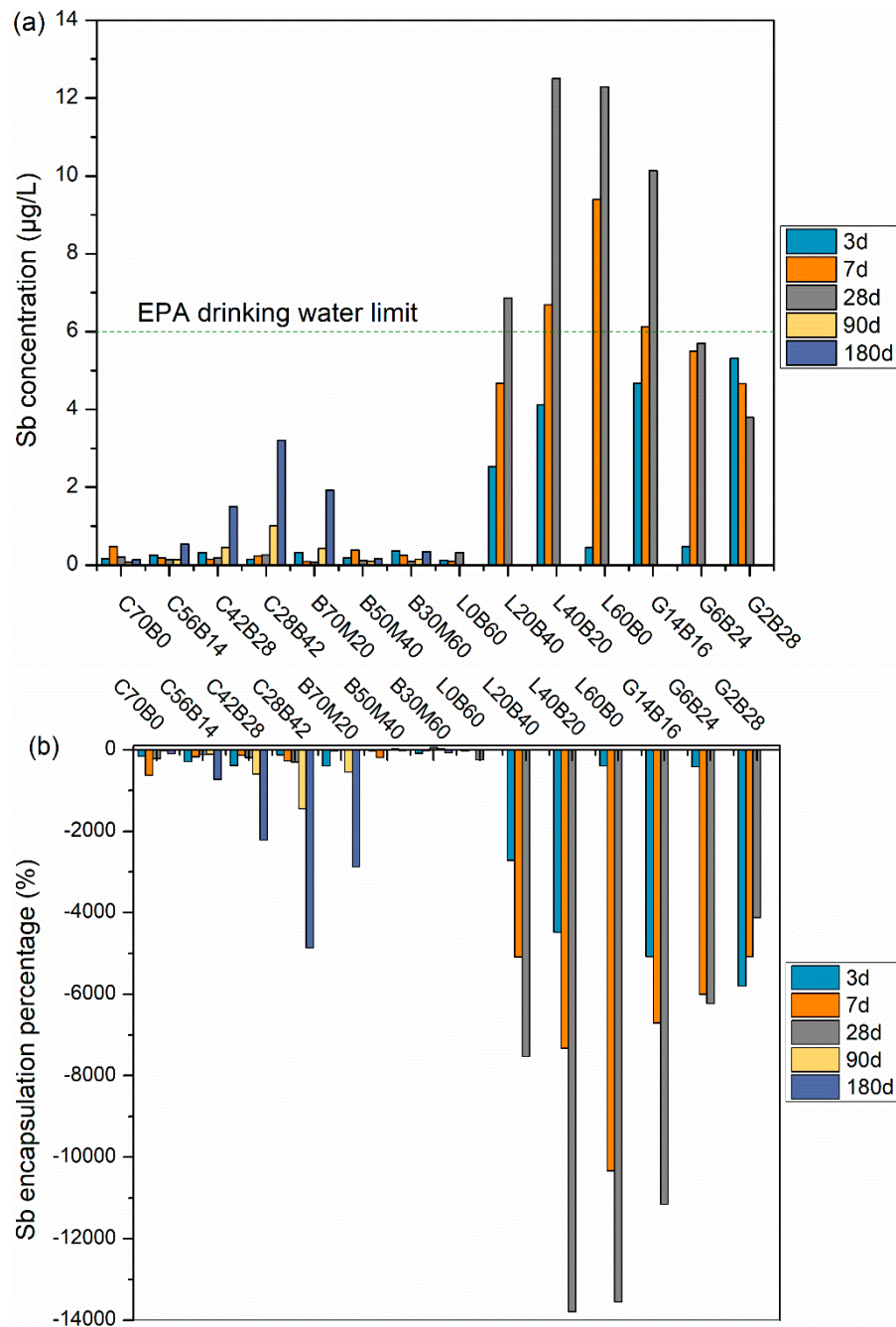


Figure 9. The (a) Sb concentration and (b) encapsulation percentage for the leachate in all groups at all ages.

3.3.7. The Encapsulation of Cd

Figure 10 shows the Cd concentrations and the encapsulation percentage at all ages for all groups. All mixtures show Cd amounts below the EPA drinking water limit, in contrast with the MSWIFA and

water mixture, which shows values slightly greater than the limit. All groups show an encapsulation percentage greater than 70%, with the BM and CB groups showing lower percentages than the other groups. It can be inferred that LFS helps with Cd stabilization. Due to the low concentrations, there could be some fluctuations and errors in the data. Cd encapsulation in this study is in agreement with the literature [1,6,7,11,22,32,34,35,41,48]. The incorporation of bivalent ions, such as Cd^{2+} , is possible in the structure of calcium sulfoaluminates such as Friedel's salt and ettringite, for example by ionic substitution of calcium [22]. The surface compound for Cd has been identified as the mixed hydroxide $\text{CaCd}(\text{OH})_4$ [32]. Cd^{2+} can also be incorporated in C-S-H gel either physically or through surface adsorption [7].

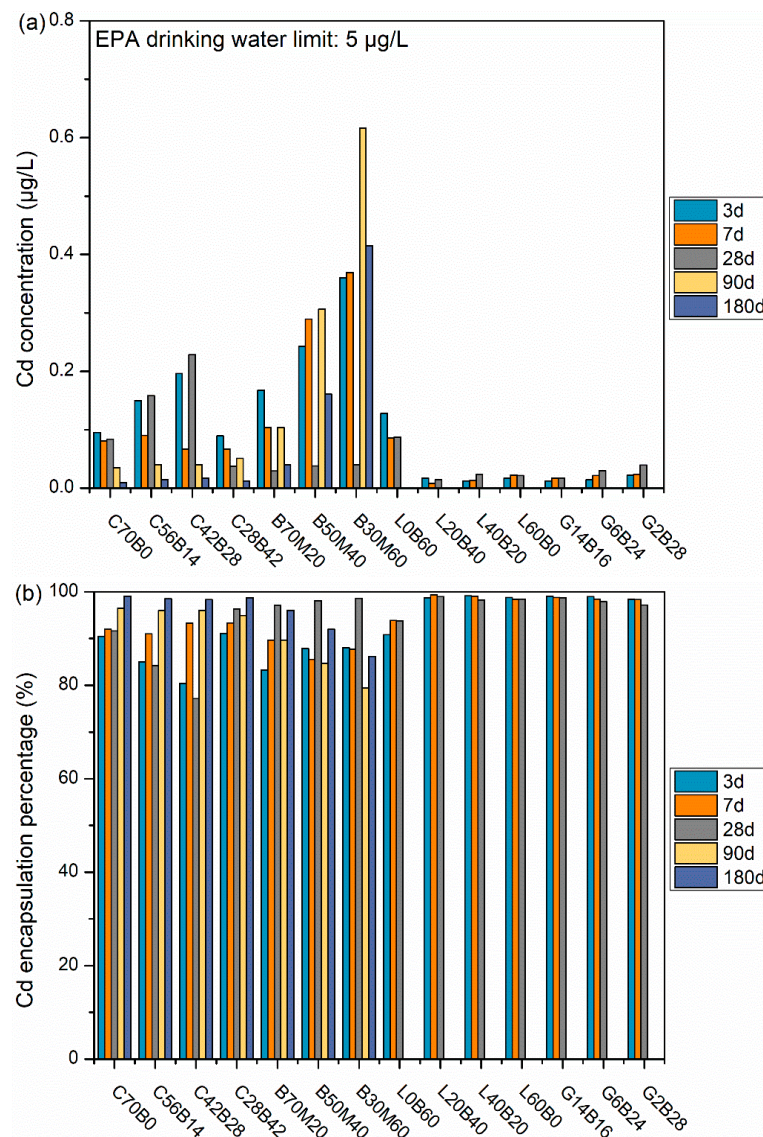


Figure 10. The (a) Cd concentration and (b) encapsulation percentage for the leachate in all groups at all ages.

3.3.8. The Encapsulation of Hg

The Hg concentrations and the encapsulation percentage at all ages for all groups are presented in Figure 11. Except for one group at 3 days, all mixtures show concentration values below the EPA limit. At later ages, the mixtures show values significantly below the limit, in contrast with the MSWIFA–water mixture, which shows a value close to the limit. The groups showing high Hg values

at 3 days show Hg leaching, but, after 7 days, all groups have some Hg encapsulation. Due to the low concentration values, there could be some fluctuation and error in the data. Mixtures with LFS show relatively poor performance compared to other mixtures. Hg encapsulation performance is in good agreement with the literature [6,9]. HgO is expected to form in highly alkaline pore solutions with cement, and it can be physically encapsulated in the hydrates. Complex precipitation or the formation of solid solutions may need to be considered [32].

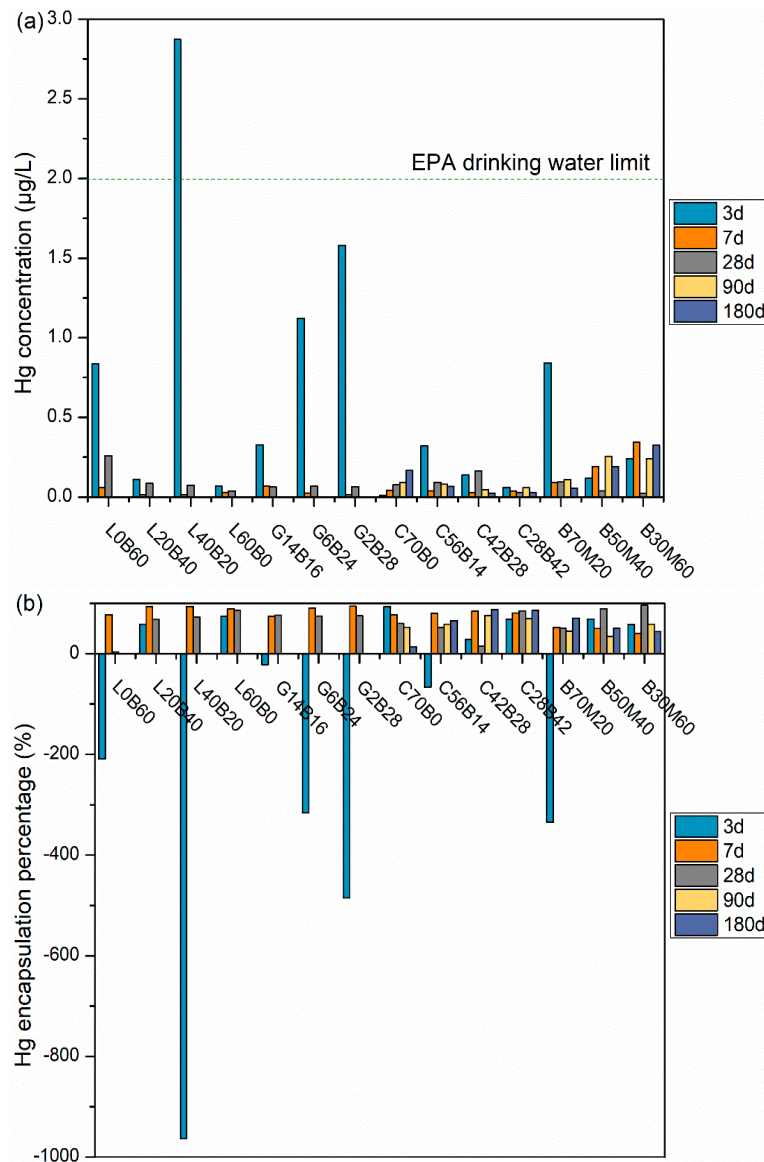


Figure 11. The (a) Hg concentration and (b) encapsulation percentage for the leachate in all groups at all ages.

3.3.9. The Performance of Mixtures B50M40 and B30M60

For mixtures B50M40 and B30M60 with large amounts of MSWIFA in the mixture, the encapsulation percentage is in general higher than other mixtures in groups BM and CB at early ages but is almost the same as the other mixtures at later ages. This is because the original metal concentration of these two systems is higher, which may lead to a higher encapsulation percentage. When considering the absolute concentration, the values in these groups are generally higher than other groups due to the larger amount of MSWIFA in the system.

3.4. Summary of Encapsulation Performance

For all mixtures, the encapsulation percentage is generally higher at later ages. The encapsulation process requires time and generally proceeds as hydration proceeds. As hydration proceeds, greater amounts of hydrates are formed, the microstructure is densified, and the porosity is reduced; all of these lead to greater encapsulation. Table 4 below shows the encapsulation performance for each heavy metal for all groups.

Table 4. The encapsulation performance for each heavy metal for all groups. The notations are as follows—C: leachate concentration; P: encapsulation percentage; √: within EPA drinking water limit; ×: exceeds EPA drinking water limit; *: encapsulation percentage varies significantly over time (generally increases); -: not applicable.

Mixture.	Cr		Cu		Zn		Pb		Sb		Cd		Hg	
	C	P	C	P	C	P	C	P	C	P	C	P	C	P
MSWIFA + Water	×	-	-	-	-	-	×	-	-	-	-	-	×	-
C70B0														
C56B14														
C42B28		*												
C28B42									√					
B70M20			√	*	√	>90%		>90%		<60%	√	>60%	√	*
B50M40														
B30M60	√													
L0B60							√							
L20B40														
L40B20									×				×	
L60B0		>90%												
G14B16												>90%		
G6B24													√	
G2B28									√					

When considering all ions, concentrations of Cr, Cu, Zn and Cd never cross the EPA drinking water limit at any age. Cd, Pb and Zn are efficiently encapsulated for the entire testing period. Some metals such as Cr, Cu and Hg go through an “induction period” of low encapsulation at early ages but have a significant enhancement of the encapsulation at later ages. High pH environment appears to lead to the leaching of Sb and Pb.

When considering the developed mixtures, C70B0, L20B40, L40B20, L60B0 and G14B16 exceed EPA drinking water limit for one or more heavy metals. The heavy metals of concern are Pb for C70B0, Hg for L40B20, and Sb for L20B40, L40B20, L60B0 and G14B16. The other mixtures safely encapsulate all heavy metal concentrations. It should be noted that while mixtures with LFS generally show the best encapsulation, most mixtures with LFS fail to adequately encapsulate Sb and therefore are not suggested for MSWIFA encapsulation.

3.5. Encapsulation and Hydrate Nature

Several mixtures show excellent encapsulation behavior. While mixtures containing LFS generally show greater encapsulation than other mixtures, they perform very poorly in encapsulating Sb. The calcium aluminates, such as mayenite, in LFS enhance heavy metal encapsulation due to the formation of large amounts of LDH phases.

The major hydrates formed in the mixtures that play a role in encapsulation are Friedel’s salt, ettringite, and C-S-H. Friedel’s salt shows significant ionic substitutions at its aluminum and sulfate sites. The aluminum site can accommodate different trivalent and tetravalent cations in varying proportions. Monovalent and divalent anions and cations may also be incorporated in

these phases [2,8,10,14,17,22,34,35,41,45,49]. The uptake of divalent metal cations in these phases occurs through the precipitation of the metal hydroxides on the surfaces, intercalation by structural incorporation, and adsorption by the surface hydroxyl groups [17,49]. Ettringite can act as a host to numerous ions, including Ca^{2+} , Al^{3+} , SO_4^{2-} and OH^- , through chemical substitution in both the column and channel sections of its structure [9]. C-S-H can also host a number of heavy metals in both ionic and salt form. Immobilization mechanisms of C-S-H include adsorption, physical wrapping, and ionic substitution. As the amount of Al in mixtures increases, the amount of Al in the C-S-H can also increase, which may lead to encapsulation of greater amounts of heavy metals [45].

Table 5 shows the main hydrates and encapsulation mechanisms of representative mixtures.

Table 5. Major hydrates and encapsulation mechanisms of representative mixtures.

Mixtures	Major Hydrates	Encapsulation Mechanisms	Comments
C70B0	C-S-H	Physical encapsulation and adsorption	Pb exceeds EPA limit. Encapsulation high for Zn, Cd.
C42B28	C-S-H	Physical encapsulation and adsorption	All ions below EPA limit. Encapsulation high for Zn, Pb.
B70M20	C-S-H	Physical encapsulation and adsorption	All ions below EPA limit. Encapsulation high for Zn, Pb.
B30M60	Friedel's salt and C-S-H	Ionic substitution, phase mixing and adsorption	All ions below EPA limit. Encapsulation high for Zn, Pb.
L40B20	Friedel's salt and Ettringite	Ionic substitution and adsorption	Sb, Hg exceed EPA limit. Encapsulation high for Cr, Zn, Pb and Cd.
L60B0	Friedel's salt	Ionic substitution and adsorption	Sb exceeds EPA limit. Encapsulation high for Cr, Zn, Pb and Cd.
G2B28	Friedel's salt	Ionic substitution and adsorption	All ions below EPA limit. Encapsulation high for Cr, Zn, Pb and Cd.

Among the mixtures tested, mixtures C56B14, C42B28, C28B42 and B70M20 never exceed EPA drinking water limits for any heavy metal and show adequate early compressive strength (above 20 MPa at 3 days). While mixtures with LFS generally show high encapsulation, they show poor performance with Sb (EPA drinking water limit is exceeded). In addition, several mixtures with LFS show poor early strength (below 10 MPa at 3 days). Therefore, if one were to use zero cement mixtures for MSWIFA encapsulation, the mixture B70M20 would be ideal, but the mixtures with LFS would not.

4. Conclusions

In this paper, compressive strength, X-ray diffraction (XRD), and leaching tests were performed to understand the hydration processes, compressive strength evolution, and heavy metal encapsulation in municipal solid waste incineration fly ash (MSWIFA) pastes with varying amounts of ladle furnace slag (LFS), ground granulated blast-furnace slag (GGBFS), cement, and flue gas desulfurization (FGD) gypsum. The predominant hydration products in these systems are Friedel's salt, ettringite, and C-S-H. Mixtures with high amounts of LFS or MSWIFA have poor early-age strength. This low early-age strength is attributed to several reasons including deleterious agents in LFS and MSWIFA. Mixtures with optimum combinations of cement and GGBFS gain the highest strength. In mixtures with large amount of LFS, the principle hydration products are C-S-H gel and Friedel's salt, while the primary hydration products of mixtures without LFS are C-S-H gel and ettringite. Mixtures with excessive MSWIFA form Friedel's salt because of the large amount of chloride in the system. Cr, Cu, Zn and Cd are safely encapsulated in all mixtures with the concentration of the leachate under the EPA drinking water limit. Zn, Pb and Cd show similarly high encapsulation during the testing period while Cr, Cu and Hg show increasing encapsulation with age. Most heavy metals showed increasing encapsulation with increases in LFS amounts due to calcium aluminate hydrate phase formation with the notable exception of Sb. LFS mixtures show poor Sb encapsulation, and most mixtures show Sb leaching. Among the tested mixtures, mixtures C56B14, C42B28, C28B42 and B70M20 are ideal as they satisfy both leaching and strength requirements. The only zero cement mixture that shows satisfactory behavior is B70M20.

Author Contributions: Conceptualization, Y.W. and W.N.; methodology, Y.W, W.N, S.Z., and J.L.; formal analysis, Y.W, W.N, S.Z., J.L., and P.S.; writing—original draft preparation, Y.W.; writing—review and editing, Y.W, W.N,

S.Z., J.L., and P.S.; funding acquisition, W.N. All authors have read and agreed to the published version of the manuscript.

Funding: This research was funded by the Ministry of Science and Technology of the People's Republic of China (NO. 2019YFC1803500).

Acknowledgments: The authors would like to acknowledge Yijie Wang at the University of Science and Technology Beijing for help in performing some experiments.

Conflicts of Interest: The authors declare no conflict of interest.

References

1. Du, B.; Li, J.; Fang, W.; Liu, J. Comparison of long-term stability under natural ageing between cement solidified and chelator-stabilised MSWI fly ash. *Environ. Pollut.* **2019**, *250*, 68–78. [\[CrossRef\]](#) [\[PubMed\]](#)
2. Fan, C.; Wang, B.; Zhang, T. Review on cement stabilization/solidification of municipal solid waste incineration fly ash. *Adv. Mater. Sci. Eng.* **2018**, *2018*. [\[CrossRef\]](#)
3. Guo, X.; Hu, W.; Shi, H. Microstructure and self-solidification/stabilization (S/S) of heavy metals of nano-modified CFA–MSWIFA composite geopolymers. *Constr. Build. Mater.* **2014**, *56*, 81–86. [\[CrossRef\]](#)
4. Ho, H.; Chow, J.; Gau, S. Thermal mobility of heavy metals in municipal solid waste incinerator fly ash (MSWIFA). *Environ. Eng. Sci.* **2008**, *25*, 649–656. [\[CrossRef\]](#)
5. Saikia, N.; Kato, S.; Kojima, T. Production of cement clinkers from municipal solid waste incineration (MSWI) fly ash. *Waste Manag.* **2007**, *27*, 1178–1189. [\[CrossRef\]](#)
6. Quina, M.J.; Bordado, J.C.; Quinta-Ferreira, R.M. Treatment and use of air pollution control residues from MSW incineration: An overview. *Waste Manag.* **2008**, *28*, 2097–2121. [\[CrossRef\]](#)
7. Wang, K.; Ni, W.; Zhang, S. Stabilization/Solidification of cadmium in municipal solid waste incineration fly ash by using cemented backfill agent. In *IOP Conference Series: Earth and Environmental Science*; IOP Publishing: Hefei, China, 2019. [\[CrossRef\]](#)
8. Wang, L.; Cho, D.W.; Tsang, D.C.W.; Cao, X.; Hou, D.; Shen, Z.; Alessi, D.S.; Ok, Y.S.; Poon, C.S. Green remediation of As and Pb contaminated soil using cement-free clay-based stabilization/solidification. *Environ. Int.* **2019**, *126*, 336–345. [\[CrossRef\]](#)
9. Gougar, M.L.D.; Scheetz, B.E.; Roy, D.M. Ettringite and C-S-H Portland cement phases for waste ion immobilization: A review. *Waste Manag.* **1996**, *16*, 295–303. [\[CrossRef\]](#)
10. Rha, C.Y.; Kang, S.K.; Kim, C.E. Investigation of the stability of hardened slag paste for the stabilization/solidification of wastes containing heavy metal ions. *J. Hazard. Mater.* **2000**, *73*, 255–267. [\[CrossRef\]](#)
11. Deja, J. Immobilization of Cr^{6+} , Cd^{2+} , Zn^{2+} and Pb^{2+} in alkali-activated slag binders. *Cem. Concr. Res.* **2002**, *32*, 1971–1979. [\[CrossRef\]](#)
12. Saikia, N.; Cornelis, G.; Mertens, G.; Elsen, J.; Balen, K.V.; Gerven, T.V.; Vandecasteele, C. Assessment of Pb-slag, MSWI bottom ash and boiler and fly ash for using as a fine aggregate in cement mortar. *J. Hazard. Mater.* **2008**, *154*, 766–777. [\[CrossRef\]](#) [\[PubMed\]](#)
13. Guo, X.; Shi, H. Utilization of steel slag powder as a combined admixture with ground granulated blast-furnace slag in cement-based materials. *J. Mater. Civ. Eng.* **2013**, *25*, 1990–1993. [\[CrossRef\]](#)
14. Li, C.; Sun, H.; Li, L. A review: The comparison between alkali-activated slag (Si+Ca) and metakaolin (Si+Al) cements. *Cem. Concr. Res.* **2010**, *40*, 1341–1349. [\[CrossRef\]](#)
15. Wang, Y.; Suraneni, P. Experimental methods to determine the feasibility of steel slags as supplementary cementitious materials. *Constr. Build. Mater.* **2019**, *204*, 458–467. [\[CrossRef\]](#)
16. Yan, A.; Ni, W.; Huang, X.; Zhang, J.; Li, Y.; Xu, D. Solidification/stabilization of Pb^{2+} within a blast furnace slag-steel slag based cementing agent for paste backfilling. *J. Univ. Sci. Technol. Beijing* **2016**, *7*, 899–905.
17. Yoon, H.N.; Seo, J.; Kim, S.; Lee, H.K.; Park, S. Characterization of blast furnace slag-blended Portland cement for immobilization of Co. *Constr. Build. Mater.* **2020**, *134*, 106089. [\[CrossRef\]](#)
18. Zhang, Y.; Sun, W.; Chen, Q.; Chen, L. Synthesis and heavy metal immobilization behaviors of slag based geopolymer. *J. Hazard. Mater.* **2007**, *143*, 206–213. [\[CrossRef\]](#)
19. Zhang, Y.; Gao, W.; Ni, W.; Zhang, S.; Li, Y.; Wang, K.; Huang, X.; Fu, P.; Hu, W. Influence of calcium hydroxide addition on arsenic leaching and solidification/stabilisation behaviour of metallurgical-slag-based green mining fill. *J. Hazard. Mater.* **2020**, *390*, 122161. [\[CrossRef\]](#)

20. Lončnar, M.; Van der Sloot, H.A.; Mladenović, A.; Zupančič, M.; Kobal, L.; Bukovec, P. Study of the leaching behaviour of ladle slags by means of leaching tests combined with geochemical modelling and mineralogical investigations. *J. Hazard. Mater.* **2016**, *317*, 147–157. [\[CrossRef\]](#)
21. Wang, Y.; Ni, W.; Suraneni, P. Use of ladle furnace slag and other industrial by-products to encapsulate chloride in municipal solid waste incineration fly ash. *Materials* **2019**, *12*, 925. [\[CrossRef\]](#)
22. Giergiczny, Z.; Król, A. Immobilization of heavy metals (Pb, Cu, Cr, Zn, Cd, Mn) in the mineral additions containing concrete composites. *J. Hazard. Mater.* **2008**, *160*, 247–255. [\[CrossRef\]](#) [\[PubMed\]](#)
23. Cyr, M.; Idir, R.; Escadeillas, G. Use of metakaolin to stabilize sewage sludge ash and municipal solid waste incineration fly ash in cement-based materials. *J. Hazard. Mater.* **2012**, *243*, 193–203. [\[CrossRef\]](#) [\[PubMed\]](#)
24. Wan, S.; Zhou, X.; Zhou, M.; Han, Y.; Chen, Y.; Geng, J.; Wang, T.; Xu, S.; Qiu, Z.; Hou, H. Hydration characteristics and modeling of ternary system of municipal solid wastes incineration fly ash-blast furnace slag-cement. *Constr. Build. Mater.* **2018**, *180*, 154–166. [\[CrossRef\]](#)
25. Sheshukov, O.; Yu, O.; Nerkasov, I.V.; Mikheenkova, M.A.; Egiazaryan, D.K.; Sivtsov, A.V.; Chencov, V.P.; Gertsberg, G.E. Unit ladle-furnace: Slag forming conditions and stabilization. *KnE Mater. Sci.* **2017**, *70*–75. [\[CrossRef\]](#)
26. Rađenović, A.; Malina, J.; Sofilić, T. Characterization of ladle furnace slag from carbon steel production as a potential adsorbent. *Adv. Mater. Sci. Eng.* **2013**, *2013*. [\[CrossRef\]](#)
27. Chaunsali, P.; Peethamparan, S. Evolution of strength, microstructure and mineralogical composition of a CKD–GGBFS binder. *Cem. Concr. Res.* **2011**, *41*, 197–208. [\[CrossRef\]](#)
28. Van der Sloot, H.A. Characterization of the leaching behaviour of concrete mortars and of cement-stabilized wastes with different waste loading for long term environmental assessment. *Waste Manag.* **2002**, *22*, 181–186. [\[CrossRef\]](#)
29. Bendz, D.; Pascal, S.; Van der Sloot, H.; Kosson, D.; Flyhammar, P. *Modelling of Leaching and Geochemical Processes in an Aged MSWIBA Subbase Layer*; Värmeforsk Service AB: Stockholm, Sweden, 2009.
30. Fregert, S.; Gruvberger, B. Chemical aspects on chromate in cement. *Dermatosen in Beruf und Umwelt. Occup. Environ.* **1982**, *30*, 76–78.
31. Estokova, A.; Palascakova, L.; Kanuchova, M. Study on Cr (VI) leaching from cement and cement composites. *Int. J. of Environ. Res. Public Health* **2018**, *15*, 824. [\[CrossRef\]](#)
32. Gress, D.L.; El-Korchi, T. *Microstructural Characterisation of Cement-Solidified Heavy Metal Wastes*; Lewis Publishers: Washington, DC, USA, 1991.
33. Kanchinadham, S.B.K.; Narasimman, L.M.; Pedaballe, V.; Kalyanaraman, C. Diffusion and leachability index studies on stabilization of chromium contaminated soil using fly ash. *J. Hazard. Mater.* **2015**, *297*, 52–58. [\[CrossRef\]](#)
34. Peysson, S.; Péra, J.; Chabannet, M. Immobilization of heavy metals by calcium sulfoaluminate cement. *Cem. Concr. Res.* **2005**, *35*, 2261–2270. [\[CrossRef\]](#)
35. Qian, G.; Cao, Y.; Chui, P.; Tay, J. Utilization of MSWI fly ash for stabilization/solidification of industrial waste sludge. *J. Hazard. Mater.* **2006**, *129*, 274–281. [\[CrossRef\]](#) [\[PubMed\]](#)
36. Tian, X.; Li, C.; Zhao, F.; Liu, Z. Study on properties of steel slag-blast furnace slag-zeolite binder for solidification/stabilization of heavy metals. In *IOP Conference Series: Earth and Environmental Science*; IOP Publishing: Bristol, England, 2009. [\[CrossRef\]](#)
37. Li, X.D.; Poon, C.S.; Sun, H.; Lo, I.M.C.; Kirk, D.W. Heavy metal speciation and leaching behaviors in cement based solidified/stabilized waste materials. *J. Hazard. Mater.* **2001**, *82*, 215–230. [\[CrossRef\]](#)
38. Weeks, C.; Hand, R.J.; Sharp, J.H. Retardation of cement hydration caused by heavy metals present in ISF slag used as aggregate. *Cem. Concr. Compos.* **2008**, *30*, 970–978. [\[CrossRef\]](#)
39. Pierrard, J.C.; Rimbault, J.; Aplincourt, M. Experimental study and modelling of lead solubility as a function of pH in mixtures of ground waters and cement waters. *Water Res.* **2002**, *36*, 879–890. [\[CrossRef\]](#)
40. Xie, Y. Dissolution, formation, and transformation of the lead corrosion product PbO₂: Rates and mechanisms of reactions that control lead release in drinking water distribution systems. Ph.D. Thesis, Washington University, St. Louis, MO, USA, 2010. Available online: <https://openscholarship.wustl.edu/etd/387/> (accessed on 1 January 2020).
41. Cartledge, F.K.; Butler, L.G.; Chalasani, D.; Eaton, H.C.; Frey, F.P.; Herrera, E.; Tittlebaum, M.E.; Yang, S.L. Immobilization mechanisms in solidification/stabilization of cadmium and lead salts using portland cement fixing agents. *Environ. Sci. Technol.* **1990**, *24*, 867–873. [\[CrossRef\]](#)

42. Moon, D.H.; Dermatas, D. An evaluation of lead leachability from stabilized/solidified soils under modified semi-dynamic leaching conditions. *Eng. Geol.* **2006**, *85*, 67–74. [[CrossRef](#)]
43. Palomo, A.; Palacios, M. Alkali-activated cementitious materials: Alternative matrices for the immobilisation of hazardous wastes: Part II. Stabilisation of chromium and lead. *Cem. Concr. Res.* **2003**, *33*, 289–295. [[CrossRef](#)]
44. Gao, W.; Ni, W.; Zhang, Y.; Li, Y.; Shi, T.; Li, Z. Investigation into the semi-dynamic leaching characteristics of arsenic and antimony from solidified/stabilized tailings using metallurgical slag-based binders. *J. Hazard. Mater.* **2020**, *381*, 120992. [[CrossRef](#)]
45. Kiventerä, J.; Lancellotti, I.; Catauro, M.; Poggetto, F.D.; Leonelli, C.; Illikainen, M. Alkali activation as new option for gold mine tailings inertization. *J. Clean. Prod.* **2018**, *187*, 76–84. [[CrossRef](#)]
46. Kiventerä, J.; Sreenivasan, H.; Cheeseman, C.; Kinnunen, P.; Illikainen, M. Immobilization of sulfates and heavy metals in gold mine tailings by sodium silicate and hydrated lime. *J. Environ. Chem. Eng.* **2018**, *6*, 6530–6536. [[CrossRef](#)]
47. Zhang, Y.; Zhang, S.; Ni, W.; Yan, Q.; Gao, W.; Li, Y. Immobilisation of high-arsenic-containing tailings by using metallurgical slag-cementing materials. *Chemosphere* **2019**, *223*, 117–123. [[CrossRef](#)] [[PubMed](#)]
48. Saikia, N.; Brito, J. Use of industrial waste and municipality solid waste as aggregate, filler or fiber in cement mortar and concrete. *Adv. Mater. Sci. Res.* **2009**, *3*, 65–116.
49. Zhang, M.; Reardon, E.J. Chromate and selenate hydrocalumite solid solutions and their applications in waste treatment. *Sci. China Ser. C Life Sci.* **2005**, *48*, 165–173. [[CrossRef](#)]



© 2020 by the authors. Licensee MDPI, Basel, Switzerland. This article is an open access article distributed under the terms and conditions of the Creative Commons Attribution (CC BY) license (<http://creativecommons.org/licenses/by/4.0/>).